Antiferromagnetic Spatial Ordering in a Quenched One-Dimensional Spinor Gas

A. Vinit, E. M. Bookjans, C. A. R. Sá de Melo, and C. Raman[*]

School of Physics, Georgia Institute of Technology, Atlanta, Georgia 30332, USA
(Received 19 September 2012; revised manuscript received 10 December 2012; published 15 April 2013)

We have experimentally observed the emergence of spontaneous antiferromagnetic spatial order in a sodium spinor Bose-Einstein condensate that was quenched through a magnetic phase transition. For negative values of the quadratic Zeeman shift, a gas initially prepared in the $F = 1$, $m_F = 0$ state collapsed into a dynamically evolving superposition of all three spin projections, $m_F = 0$, ± 1. The quench gave rise to rich, nonequilibrium behavior where both nematic and magnetic spin waves were generated. We characterized the spatiotemporal evolution through two particle correlations between atoms in each pair of spin states. These revealed dramatic differences between the dynamics of the spin correlations and those of the spin populations.

Dynamics far from equilibrium occur ubiquitously in nature. A prime example can be found close to a symmetry breaking phase transition. A rapid passage through the critical point can quickly nucleate spatial inhomogeneities that subsequently evolve slowly with time. Such behavior typifies physical systems of vastly different microscopic origin, for example, rapid cooling of the early Universe following inflation [1–3], the chiral symmetry breaking phase transition in heavy-ion collisions [4,5], and sudden cooling of solid-state magnets below the Curie temperature [6]. The nature of the pattern formation is of fundamental interest to uncover its universal features [7,8]. For example, the temporal evolution of correlation functions can yield critical exponents of the phase transition [9]. Understanding how entanglement and correlations flow in a many-body system is also relevant for enabling quantum computation [10].

The spin degrees of freedom of a Bose gas offer exciting possibilities for the exploration of nonequilibrium phenomena [11–15]. In this work we have realized a quantum quench in the laboratory by crossing through a magnetic phase transition in an antiferromagnetic, $F = 1$ sodium spinor Bose-Einstein condensate (BEC), as shown in Fig. 1. We have captured the stochastic dynamics of this quench through spatially resolved measurements of two particle spin correlations. The spin-dependent mean-field Hamiltonian,

$$H_{\mathrm{sp}} = c_2 n \langle \hat{\mathbf{F}} \rangle^2 + q \langle \hat{F}_z^2 \rangle,$$

contains a competition between intrinsic magnetic interactions and the coupling to an external magnetic field. The latter is parametrized by the quadratic Zeeman shift q, which we rapidly switched from positive to negative values to initiate the quench. Similar correlation measurements have been performed recently for quenched superfluids without spin [16,17]. In the above formula, n is the mean particle density and c_2 is the strength of spin-dependent interactions, which can be either positive (for

antiferromagnets) or negative (for ferromagnets). $\hat{\mathbf{F}}$ and $\hat{F}_z$ are the vector spin 1 operator and its $\hat{z}$ projection, respectively. A variety of quantum phases can be realized depending on the value of q [11]. In $F = 1$ ^{87}Rb, where $c_2 < 0$, altering q suddenly through a phase boundary resulted in spontaneous transverse magnetization patterns [18].

The case $c_2 > 0$ has been much less studied. Here it is nematic, rather than magnetic, order that is the principal degree of freedom [19–23], which profoundly affects the nature of the spatial patterns and their dynamics [24]. Early work on antiferromagnetic gases principally explored instabilities in two spin components, where nematic order played no role [25]. In our experiment, we observe spatial dynamics after tuning q through a phase transition at $q = 0$ using microwave magnetic fields, a transition first observed in our earlier work [26]. Related work on $F = 2$ ^{87}Rb BEC, for which $c_2 > 0$, triggered pattern formation at a specific wavelength by preparing an unstable initial state [27]. Our work explores complementary dynamics, where passage through a phase transition generates fluctuations in the nematic order on all length scales rather than just a specific wave vector as in Ref. [27]. Thus the path to equilibrium involves the collective dynamics of *many* modes, which is our focus.

We used time-of-flight Stern-Gerlach (TOF SG) observation to record the one-dimensional spatiotemporal pattern formation in all three spin components, $m_F = 0$, ± 1, with high resolution. This method works only for extreme aspect ratio traps [28]. Importantly, we also resolved the spin density *fluctuations*, which revealed the crucial role played by the spin-mixing interaction between atom pairs, $2(m_F = 0) \leftrightarrow (m_F = 1) + (m_F = -1)$. This interaction leads to entanglement between spins [29–31], and to density correlations since the fluctuations are simply related by $\Delta n_0 = -2\Delta n_{-1} = -2\Delta n_{+1}$. In our experiment we show these to initially develop *locally*, and then to evolve *globally*. We have spatially resolved the full spin-density correlation matrix of a quantum quench, to our knowledge, for
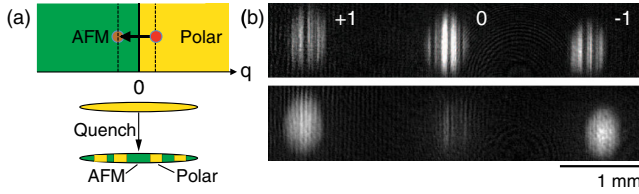
FIG. 1 (color online). Quantum quench dynamics.
(a) Instantaneous change in quadratic Zeeman energy q brings
the gas through a phase transition between polar ($m_F = 0$) and
antiferromagnetic (AFM) ($m_F = \pm 1$) ground states at $t = 0$.
Elongated BEC (yellow ellipse) subsequently develops one-
dimensional spin domains. (b) Time-of-flight Stern-Gerlach
images show the spontaneous axial spin structures at a hold
time of 48 ms (upper image, $q = h \times -4.2$ Hz) while by 2.5 s
(lower image, $q = h \times -1.7$ Hz) the system has relaxed to an
antiferromagnetic configuration free of domains. Residual
fringes in the latter image are experimental artifacts due to the
probe light.

the first time. In thermal equilibrium these density corre-
lations directly determine the compressibility matrix
[32,33].

Optically confined Bose-Einstein condensates in the
$m_F = 0$ state were prepared in a static magnetic field
of $B_x = 100$ mG in a manner described in our earlier
work [26]. Transverse magnetic fields and field gradients
were compensated to within 5 mG and 0.6 mG/cm,
respectively. The peak density $n_0 = 5 \times 10^{14}$ cm^{-3} and
axial Thomas-Fermi radius $R_x = 340$ μm were mea-
sured to an accuracy of 5%, from which we deter-
mined the spin-dependent interaction energy $c_2 n_0 = h \times$
120 Hz. The axial and radial trapping frequencies were 7
and 470 Hz, respectively, accurate to 10%. The radial
Thomas-Fermi radius, $R_\perp = 5$ μm, was small enough
such that only axial spin domains could form [34]. The
measured temperature was 400 nK, close to the chemical
potential of 360 nK.

We rapidly switched q from $q_i = h \times +2.8$ Hz > 0 to a
final value $q_f = h \times -4.2$ Hz < 0 at $t = 0$. A quantum
phase transition divides the polar ($m_F = 0$) ground state
from an "antiferromagnetic" one ($m_F = \pm 1$ superposi-
tion) at $q = 0$, as shown in Fig. 1. The dynamical evolution
from one to the other state is governed by the spin-
dependent interaction term $\propto c_2$. q was switched by turn-
ing on a far-off resonance microwave "dressing" field
tuned to near the $F = 1 \to F = 2$ ground state hyperfine
resonance. The value of q_f was controlled through the ac
Stark shift by adjusting the microwave power [35].

Since $q_i, |q_f| \ll c_2 n_0$, the gas remained very close to
the phase transition point at all times. Nonetheless, the
change triggered a rapid instability in the $m_F = 0$ conden-
sate. Through spin exchange collisional interactions we
observed that the $m_F = \pm 1$ population fraction f_{pm}
increased rapidly starting at $t = 20$ ms [see Fig. 4(b)].
This was accompanied by oscillations and a slower period

of relaxation over >100 ms toward an apparent equilib-
rium. We observed a 30% atom loss over 100 ms due to off
resonant microwave excitation.

After holding the gas for a time t, the initial spin density
fluctuations were amplified, and ultimately, macroscopic,
one-dimensional spatial domains were observed to have
formed [see Fig. 1(b)]. We then diagnosed the axial spin
distribution using a TOF SG sequence [36] consisting
of 2 ms TOF, 4 ms pulsed SG field, and 24 ms additional
TOF to separate the three spin states, followed by a 50 μs
absorption imaging pulse on the $F = 2 \to F' = 3$ transi-
tion of the $D2$ line. Because of the extreme 70:1 aspect
ratio, the TOF axial distribution remained very close to its
in situ value. Each image was Fourier filtered to remove
spurious interference fringes with wavelength between
60–62 μm created by the probe light, and summed over
the radial direction to obtain one-dimensional atom density
distributions. We took the center of these distributions
($x = 0$) to be the maximum of the average density profile
for 30 runs at each hold time t, after smoothing by a
200 μm moving average filter.

Figure 2 shows measured spin density profiles, $n_0(x)$ and
$n_{-1}(x)$, for a single shot of the experiment at a hold time of
68 ms. Domains as small as 13 μm half width at half
maximum can be seen. This is 4% of the Thomas-Fermi
radius, and is comparable to our imaging resolution,
$d \approx 10$ μm [37]. Domains smaller than d would have
expanded to a size $\geq d$, and thus cannot be distinguished
by the time-of-flight method from larger scale features. The
energetics of the quench, however, suggest that domains no
smaller than $\hbar/(2\sqrt{Mq_f}) = 5$ μm are likely to appear.

While single images contained multiple spin domains,
the average over many runs showed no structure, indicating
that the formation and dynamics were stochastic in nature.
Therefore, we quantified the data using two-particle corre-
lations, specifically computing the two-point covariance
function for the density fluctuations Δn of a spin pair i, j,

$$S_{i,j}(x_1, x_2, t) \equiv \langle \Delta \hat{n}_i(x_1, t) \Delta \hat{n}_j(x_2, t) \rangle,$$

where $\langle \cdots \rangle$ refer to ensemble averages of fluctuations
about the sample mean, taken over 30 runs of the experi-
ment. Averages over a smaller sample size yielded similar
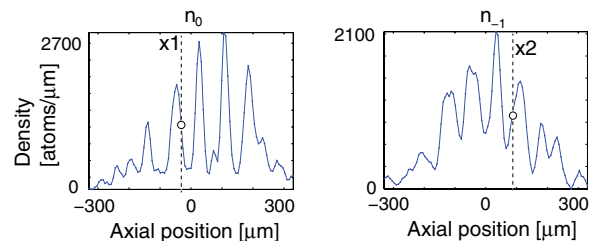results. We further analyzed these data in terms of both the

FIG. 2 (color online). Sample profiles $n_0(x)$ and $n_{-1}(x)$ mea-
sured on a single shot at $t = 68$ ms.

local correlation function ($x_1 = x_2$) and nonlocal effects ($x_1 \neq x_2$). We discuss both of these results in turn below.

Figure 3(a) shows the measured time evolution of the local pair correlation function, $R_{ij}(t) = \int dx \langle \Delta \hat{n}_i(x,t) \Delta \hat{n}_j(x,t) \rangle$. This graph is a central result of this work. Noise due to total atom number fluctuations was subtracted from the data as described later in the Letter. For short times, $t \lesssim 35$ ms, all three spin states exhibit correlations whose absolute value rises from zero to a maximum value. This is a result of the local spin mixing process discussed earlier, which predicts that the ratio $R_{1,-1}/R_{-1,-1} = 1.0$ and $R_{0,-1}/R_{-1,-1} = -2.0$. Our measured peak values of the ratios are 0.9 and -2.0, respectively. Thus our data indicate that, although the system is outside the single-mode regime [11], spin mixing generates nearly the maximum local correlations that are possible.

What is equally interesting is that for $t \gtrsim 35$ ms the data all diverge from one another. The diagonal correlations, $R_{-1,-1}$, appear to reach a steady state of 50% of their peak value. This is the result of saturation of the parametric gain due to the finite number of $m_F = 0$ atoms, which causes fluctuations in the amplified modes to be suppressed [38]. By contrast, the off-diagonal data, $R_{-1,+1}$, decay sharply. The $R_{0,-1}$ data have been scaled by the factor $-1/2$ to allow for comparison of all 3 curves, and exhibit an intermediate behavior between $R_{-1,-1}$ and $R_{+1,-1}$.

The initial, positive correlation between ± 1 atoms is indicative of nematic spin wave excitations, which are
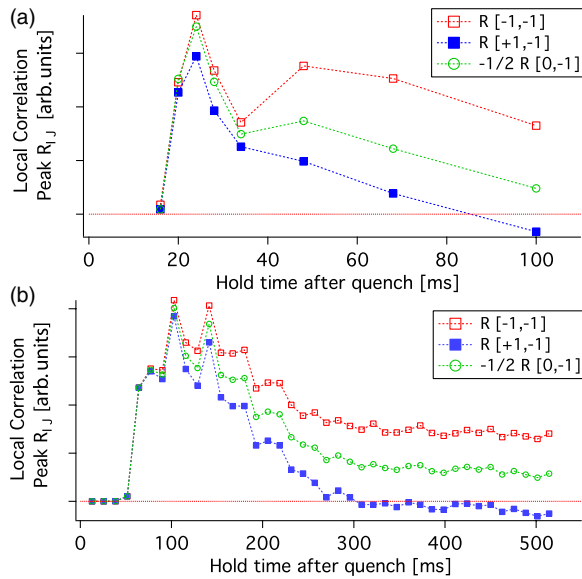

FIG. 3 (color online). Correlation of atom pairs after the quench at $t = 0$. (a) Measured local density correlations $R_{ij}(t) = \int dx \langle \Delta \hat{n}_i(x,t) \Delta \hat{n}_j(x,t) \rangle$ for spin states $(i,j) = (-1,-1)$ and $(+1,-1)$ versus time. Also shown is the $(0,-1)$ correlation scaled by a factor $-1/2$ as described in the text. (b) Correlation functions determined from numerical simulations. The horizontal dashed line marks zero correlation.
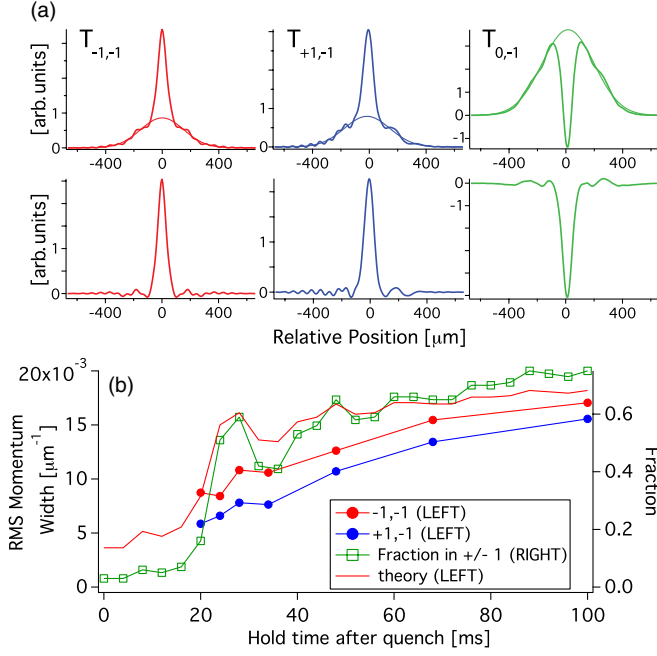
small oscillations in the order parameter $N_{zz} = n_{+1}(x,t) + n_{-1}(x,t) - 2n_0(x,t)$. These excitations occur naturally for $F = 1$ spinor condensates with $c_2 > 0$, since $m_F = 0$ regions phase separate from $m_F = \pm 1$ [36]. As time evolves, distinct regions in the condensate can communicate with one another through the propagation of these spin waves. The decay of $R_{+1,-1}$ can therefore be viewed as a destructive interference between waves originating from different points in space. Interference effects have also been recently reported in quenched scalar superfluids, leading to oscillations in the density-density correlation function [17].

Accompanying this decay of $R_{+1,-1}$ is a growth of *magnetic* spin wave excitations, whose order parameter is $M_z(x,t) = n_{+1}(x,t) - n_{-1}(x,t)$. The local magnetization variance is $\mathrm{var}[M_z(x,t)] = S_{+1,+1} + S_{-1,-1} - 2S_{-1,+1}$, which becomes nonzero for imperfect correlation between the two spins, $S_{-1,+1}(x,t) < S_{+1,+1}(x,t), S_{-1,-1}(x,t)$, as we observed experimentally. Our data in Fig. 3(a) show that $R_{+1,-1}$ reaches zero at ≈ 85 ms, after which the two spins even become negatively correlated.

In order to understand our data theoretically, we have performed numerical simulations of the three coupled spinor Gross-Pitaevskii equations. Assuming a BEC initially at zero temperature, we obtained the initial wave function for the $m_F = 0$ component numerically. Vacuum noise in the $m_F = \pm 1$ states was simulated as classical noise according to the truncated Wigner approximation [39–42]. Thirty separate simulations allowed us to compute the expectation value of quantum mechanical observables as statistical averages over different random initial conditions. Vacuum modes with wavelength less than ξ_{spin} are not expected to contribute to the spin instability. Therefore, we imposed a cutoff energy of $c_2 n_0$, which resulted in $\simeq 700$ virtual particles, while the condensate contained 5×10^6 particles, similar to the experimental conditions. The results were relatively insensitive to this cutoff, as expected for an exponential amplification process. For example, magnifying the noise by a factor of 10 changed the time at which the ± 1 fraction $= 0.5$ by only 20%.

Figure 3(b) shows the numerically obtained correlation functions, which show good qualitative agreement with the experimentally observed trends. Similar to the experimental data, $R_{+1,-1}$ has dropped below zero in the simulation after ≈ 300 ms. The overall dynamics were faster in the experiment by approximately this factor, $300/85 = 3.5$, which we cannot presently account for. Possible effects include residual ± 1 population in the initial state caused by thermal or technical fluctuations that would speed up the instability. In addition, atom loss (in our case due to off resonant microwave excitation) can cause decoherence [31].

The simulations show that, even in the absence of thermal or technical noise, vacuum fluctuations can induce a

FIG. 4 (color online). Nonlocal correlations and spin domain dynamics. (a) Top row shows $T_{i,j}(\delta) = \int S_{i,j}(x, x + \delta)dx$ for various spin pairs and relative position δ. Bottom row shows the same data with the background caused by atom number variations subtracted. (b) Dynamics of the fraction of atoms in ± 1 (green squares, right axis), the rms momentum width determined from the Fourier transform of $T_{-1,-1}$ and $T_{-1,+1}$ (red and blue circles, respectively, left axis), and from a theoretical prediction (solid red line, left axis).

decay of correlations, a somewhat counterintuitive result. For any particular realization of the experiment, the vacuum noise of the two bosonic fields, $\hat{\psi}_{+1}$ and $\hat{\psi}_{-1}$, is uncorrelated. Tiny differences in the initial conditions become amplified by the spin-mixing instability, resulting in final wave functions $\psi_{\pm 1}(t = t_F)$ that differ macroscopically, i.e., by much more than just the vacuum noise. By contrast, identical initial conditions for $\psi_{\pm 1}$ (an unphysical situation) resulted in identical time evolution and no decay, consistent with the symmetry of the Gross-Pitaevskii equations [11].

We conclude by quantifying the nonlocal dynamics. Figure 4 shows a one-dimensional reduction of the covariance map S_{ij} in terms of relative coordinate δ, $T_{i,j}(\delta, t) = \int \langle \Delta n_i(x, t) \Delta n_j(x + \delta, t) \rangle dx$, for spin pairs $(-1, -1)$, $(+1, -1)$, and $(0, -1)$, at $t = 20$ ms after the quench. A narrow peak, either positive or negative, can be seen near $\delta = 0$. A smooth, positive background lies underneath it, primarily caused by atom number variations from one shot to the next. The latter lead to correlated density fluctuations throughout the cloud [43]. The wings of the data appeared to fit well to a Gaussian distribution. When subtracted, the data revealed the *intrinsic* fluctuations, which are plotted underneath, showing a sharp, local correlation peak

surrounded by oscillations. The height of the peak was determined by an additional Gaussian fit, and constitutes the data of Fig. 3.

The oscillations signify a dynamically evolving nonlocal order induced by the rapid quench, which we characterized by computing the Fourier transforms, $T_{-1,-1}(k)$ and $T_{+1,-1}(k)$. These showed an increase in high spatial frequency components with time after the quench. Figure 4(b) shows this trend as a growth in the second moment of the Fourier transforms, $k_{\rm rms} \equiv (\int_0^\infty k^2 T dk / \int_0^\infty T dk)^{1/2}$. Higher order effects in the SG expansion are responsible for the slight magnification of $k_{\rm rms}$ for the $(-1, -1)$ relative to $(+1, -1)$.

While a rapid quench is expected to lead to coarsening of the domains on long time scales [6,44], our data show the opposite trend within the time window 0–100 ms. This suggests that it might be an intermediate phase of evolution that precedes coarsening. In fact, energy conservation requires the kinetic energy to grow with the $m_F = \pm 1$ populations, since they reduce the quadratic Zeeman energy. Using $\hbar^2 k_{\rm rms}^2 / (2M)$ from the correlation functions as an estimate of the mean kinetic energy, we obtain $\frac{k_{\rm rms}(t)}{2\pi} = \sqrt{-2Mq_f f_{\pm 1}}/h^2 = f_{\pm 1}(t)^{1/2}/(47 \ \mu{\rm m})$. This formula is plotted as a solid line Fig. 4(b) using our measurements, and shows the same trend as our data. It consistently lies above our measurements, most likely due to the fact that we do not account for variations in the phase of the order parameter nor the interaction energy contained in the finite width domain boundaries.

In summary, we have measured the time evolution of spin correlations in a quenched spinor BEC. Our data reveal rich nonequilibrium dynamics where both nematic and magnetic spin density waves are spontaneously generated. Future work will explore possible universal signatures in the decay of correlations [9].

---

*chandra.raman@physics.gatech.edu

[1] T. W. B. Kibble, J. Phys. A **9**, 1387 (1976).
[2] W. H. Zurek, Phys. Rep. **276**, 177 (1996).
[3] A. Vilenkin and E. P. S. Shellard, in *Cosmic Strings and Other Topological Defects*, Cambridge Monographs on Mathematical Physics (Cambridge University Press, Cambridge, 1994).
[4] K. Rajagopal and F. Wilczek, Nucl. Phys. **B404**, 577 (1993).
[5] B. Berdnikov and K. Rajagopal, Phys. Rev. D **61**, 105017 (2000).
[6] A. Bray, Adv. Phys. **43**, 357 (1994).
[7] A. Polkovnikov, K. Sengupta, A. Silva, and M. Vengalattore, Rev. Mod. Phys. **83**, 863 (2011).

[8] A. Lamacraft and J. Moore, in *Ultracold Bosonic and Fermionic Gases* Contemporary Concepts of Condensed Matter Science, edited by K. Levin, A. Fetter, and D. M. Stamper-Kurn (Elsevier, New York, 2012).

[9] P. Calabrese and J. Cardy, Phys. Rev. Lett. **96,** 136801 (2006).

[10] S. Bose, Contemp. Phys. **48,** 13 (2007).

[11] D. M. Stamper-Kurn and M. Ueda, arXiv:1205.1888 [Rev. Mod. Phys. (to be published)].

[12] M. Matuszewski, T. J. Alexander, and Y. S. Kivshar, Phys. Rev. A **78,** 023632 (2008).

[13] M. Matuszewski, Phys. Rev. Lett. **105,** 020405 (2010).

[14] N. T. Phuc, Y. Kawaguchi, and M. Ueda, Phys. Rev. A **84,** 043645 (2011).

[15] M. Moreno-Cardoner, J. Mur-Petit, M. Guilleumas, A. Polls, A. Sanpera, and M. Lewenstein, Phys. Rev. Lett. **99,** 020404 (2007).

[16] M. Cheneau, P. Barmettler, D. Poletti, M. Endres, P. Schausz, T. Fukuhara, C. Gross, I. Bloch, C. Kollath, and S. Kuhr, Nature (London) **481,** 484 (2012).

[17] C.-L. Hung, V. Gurarie, and C. Chin, arXiv:1209.0011.

[18] L. E. Sadler, J. M. Higbie, S. R. Leslie, M. Vengalattore, and D. M. Stamper-Kurn, Nature (London) **443,** 312 (2006).

[19] T.-L. Ho, Phys. Rev. Lett. **81,** 742 (1998).

[20] T. Ohmi and K. Machida, J. Phys. Soc. Jpn. **67,** 1822 (1998).

[21] F. Zhou, Phys. Rev. Lett. **87,** 080401 (2001).

[22] S. Mukerjee, C. Xu, and J. E. Moore, Phys. Rev. Lett. **97,** 120406 (2006).

[23] R. Barnett, J. D. Sau, and S. Das Sarma, Phys. Rev. A **82,** 031602 (2010).

[24] E. J. Mueller, Phys. Rev. A **69,** 033606 (2004).

[25] H.-J. Miesner, D. M. Stamper-Kurn, J. Stenger, S. Inouye, A. P. Chikkatur, and W. Ketterle, Phys. Rev. Lett. **82,** 2228 (1999).

[26] E. M. Bookjans, A. Vinit, and C. Raman, Phys. Rev. Lett. **107,** 195306 (2011).

[27] J. Kronjager, C. Becker, P. Soltan-Panahi, K. Bongs, and K. Sengstock, Phys. Rev. Lett. **105,** 090402 (2010).

[28] Y. Castin and R. Dum, Phys. Rev. Lett. **77,** 5315 (1996).

[29] H. Pu and P. Meystre, Phys. Rev. Lett. **85,** 3987 (2000).

[30] B. Lucke, M. Scherer, J. Kruse, L. Pezze, F. Deuretzbacher, P. Hyllus, O. Topic, J. Peise, W. Ertmer, J. Arlt *et al.*, Science **334,** 773 (2011).

[31] E. M. Bookjans, C. D. Hamley, and M. S. Chapman, Phys. Rev. Lett. **107,** 210406 (2011).

[32] K. Seo and C. A. R. Sá de Melo, arXiv:1101.3610v2.

[33] C. A. R. Sá de Melo, Phys. Rev. B **44,** 11 911 (1991).

[34] The energy available from the quench, $h \times 4$ Hz, is smaller than the transverse excitation frequency which we estimate to be $h \times 50$ Hz from a two-dimensional box model.

[35] F. Gerbier, A. Widera, S. Fölling, O. Mandel, and I. Bloch, Phys. Rev. A **73,** 041602 (2006).

[36] J. Stenger, S. Inouye, D. M. Stamper-Kurn, H.-J. Miesner, A. P. Chikkatur, and W. Ketterle, Nature (London) **396,** 345 (1998).

[37] d was determined by both the 6.6 μm camera pixel size and the blurring along the imaging axis due to the finite 300 μm radius of the expanded cloud. The latter imposed an effective resolution of 7.5 μm due to depth of focus considerations.

[38] They are not, however, reduced to zero, since the same spin state must always be correlated with itself at the same location.

[39] P. Blakie, A. Bradley, M. Davis, R. Ballagh, and C. Gardiner, Adv. Phys. **57,** 363 (2008).

[40] A. Polkovnikov, Ann. Phys. (Amsterdam) **325,** 1790 (2010).

[41] J. D. Sau, S. R. Leslie, D. M. Stamper-Kurn, and M. L. Cohen, Phys. Rev. A **80,** 023622 (2009).

[42] R. Barnett, A. Polkovnikov, and M. Vengalattore, Phys. Rev. A **84,** 023606 (2011).

[43] The area under the background was observed to largely follow the overall populations during the quench.

[44] P. C. Hohenberg and B. I. Halperin, Rev. Mod. Phys. **49,** 435 (1977).